Research article

Kimberly S. Reichel, Eva Arianna Aurelia Pogna, Simone Biasco, Leonardo Viti, Alessandra Di Gaspare, Harvey E. Beere, David A. Ritchie and Miriam S. Vitiello*

Self-mixing interferometry and near-field nanoscopy in quantum cascade random lasers at terahertz frequencies

https://doi.org/10.1515/nanoph-2020-0609
Received November 12, 2020; accepted January 31, 2021; published online March 5, 2021

Abstract: We demonstrate that electrically pumped random laser resonators, operating at terahertz (THz) frequencies, and comprising a quantum cascade laser heterostructure, can operate as sensitive photodetectors through the self-mixing effect. We devise two-dimensional cavities exploiting a disordered arrangement of surface holes that simultaneously provide optical feedback and allow light out-coupling. By reflecting the emitted light back onto the surface with random holes pattern, and by varying the external cavity length, we capture the temporal dependence of the laser voltage, collecting a rich sequence of interference fringes that follow the bias-dependent spectral emission of the laser structure. This provides a visible signature of the random laser sensitivity to the self-mixing effect, under different feedback regimes. The latter effect is then exploited, in the near-field, to demonstrate detectorless scattering near-field optical microscopy with nanoscale (120 nm) spatial resolution. The achieved results open up possibilities of detectorless speckle-free nano-imaging and quantum sensing applications across the far-infrared.

Keywords: near field nanoscopy; random lasers; self-mixing interferometry; terahertz quantum cascade lasers.

1 Introduction

Random lasers (RLs) [1, 2] rely on a highly disordered medium, supporting optical modes generated through multiple scattering processes [2, 3]. In each scattering step, photons undergo a random walk, with a particular phase, that leads to interference. This can localize light inside the laser gain region where the photons experience a longer interaction length, and light can be scattered out of the resonator with very high temporal coherence and very low spatial coherence [4].

Random lasing has been demonstrated in different architectures including: optically pumped suspended micro-particle laser dyes [5], fine powders [6], bone tissues [7] and, more recently, in electrically pumped quantum cascade lasers (QCLs), operating in the mid-IR [8] and terahertz (THz) frequency regions [9–13] of the electromagnetic spectrum.

In the last years, a broad research effort has been devoted to study and understand the rich and complex physical processes that take place in these amplifying disordered systems, including mode-locking [14] temporal distribution of photons [15], mode and Anderson localization [2], amongst many others.

A topic yet unexplored in random lasers is their sensitivity to the self-mixing (SM) effect [16, 17]. SM is based on the reinjection of a small fraction (10^{-4}–10^{-2}) of the emitted field that coherently interferes within the laser cavity. Being inherently cavity-less, the concept of intracavity reinjection in a random laser is very counterintuitive, but discloses a peculiar potential for light detection with low-noise, resulting from the low spatial coherence of the random lasers [4] and with response times set by the timescale governing the laser emission process.

Kimberly S. Reichel and Eva Arianna Aurelia Pogna are contributed equally to this work.

***Corresponding author: Miriam S. Vitiello**, NEST, CNR - Istituto Nanoscienze and Scuola Normale Superiore, Pisa 56127, Italy, E-mail: miriam.vitiello@sns.it. https://orcid.org/0000-0002-4914-0421
Kimberly S. Reichel, Eva Arianna Aurelia Pogna, Simone Biasco, Leonardo Viti and Alessandra Di Gaspare, NEST, CNR - Istituto Nanoscienze and Scuola Normale Superiore, Pisa 56127, Italy. https://orcid.org/0000-0003-4779-3549 (E.A.A. Pogna). https://orcid.org/0000-0002-1261-8575 (A. Di Gaspare)
Harvey E. Beere and David A. Ritchie, Cavendish Laboratory, University of Cambridge, Cambridge CB3 0HE, UK

Self-mixing interferometry (SMI) is a detection method where the emitted light is reinjected back into the laser cavity, usually by an external target; phase noise is generated by fluctuations of the laser frequency or of the target distance [17]. The back reflected electric field interacts coherently with the oscillating laser mode creating a modulation in all relevant laser parameters, namely, the amplitude and phase of the electric field [16–18], the carrier density [19], and the laser frequency. When the remote target is displaced, the variation of the external cavity length induces a periodic modulation of the emitted optical power and of the voltage difference across the laser terminals [16, 17]. This means that the laser can simultaneously serve as source and detector, making this technique extremely attractive for many application purposes, such as spectroscopy [20] or compact optical imaging [20–23].

Although SM in Fabry Perot QCLs have been extensively studied [19–22], and employed for many application purposes, such as tomography [23], near-field imaging [24], and spectroscopy [20], RLs provide an additional major benefit. Their low spatial coherence can indeed lead to the reduction of artifacts with clear benefits for speckle-free imaging [25, 26]. In addition, their inherently high temporal coherence [1, 2] allows the needed stability for metrological and high precision spectroscopic applications. Therefore, these devices open the possibility of detectorless speckle-free imaging in either far-field or near-field configurations, across the far infrared.

Here we demonstrate, for the first time to our knowledge, the observation of SM in RLs and exploit the latter effect to perform detectorless near-field nanoscopy experiments with a low-divergent, electrically pumped, miniaturized, continuous-wave (CW) random THz laser. To this purpose, we quantum engineer electrically pumped RLs based on surface-emitting double-metal waveguide QCLs operating at THz frequencies [12]. The QCL active material is embedded in a bi-dimensional cavity exploiting a disordered arrangement of scatterers, lithographically patterned on the top laser surface, and acting as light outcouplers. This photonic structure localizes light inside the laser gain region where the longer photons mean free path leads to large radiative losses. The specific distribution of scatterers, designed via a computer-generated algorithm, can cause either single-mode or multimode laser emission over a broad frequency bandwidth (2.7–3.5 THz) Ref. [12], therefore allowing the ability to engineer random laser emission over the spectral domain of interest. We then exploit the sensitivity of our cavity-less surface emitting resonator to SM, to implement a near-field imaging system, at THz frequencies, where a number of relevant properties best suited for such application, such as surface-emission optical coupling [12], low-divergence [12] (<10°), large optical power output (>1 mW) in CW with low power consumption (<3 W), electrical frequency tunability and/or multicolor emission, and low spatial coherence [12] can be efficiently exploited. Specifically, the reduced spatial coherence of the electrically pumped QCL RLs could be beneficial for nano-imaging applications that do not rely on coherent wavefronts, such as mapping of specific dielectric functions [27, 28] or photocurrent nanoscopy [29, 30]. Although technically demanding, this is extremely relevant in the 75–300 μm wavelength range (1–4 THz frequencies) due to fundamental resonant excitations of many molecules, solids, emerging low-dimensional materials and biological-systems [31].

2 Setup and devices

The devices investigated in the present work are electrically pumped bi-dimensional random resonators fabricated as follows.

The employed active region consists of a molecular beam epitaxy (MBE) grown GaAs/AlGaAs homogeneous heterostructure, which yields a gain profile covering the frequency region 2.7–3.4 THz. As a first step we thermally evaporate 10 nm Cr/400 nm Au onto the heterostructure surface and, simultaneously, on a 500 μm thick (n^+) Si-doped GaAs to be used as the bottom substrate; we then bond the two pieces together at the gold interfaces using a wafer bonder applying 4.5 MPa at a temperature of 360 °C for 30 min. Next, we manually lap the excess substrate of the active region until a target thickness of ~100 μm is reached. To get down to the 10 μm thick active region, we then wet etch the sample in a citric acid based solution and we remove the AlGaAs stopping layer via HF etching. We then fabricate the random resonator via a combination of three lithographic steps, by employing a laser writer. The first lithography aims to create a thin (10 nm) Cr absorbing border to suppress unwanted edge or whispering gallery modes [12]. The second lithographic step defines the top 10 nm Cr/150 nm Au contact with a random distribution of holes, having 6 μm diameter and filling factors ranging from 11% to 25%. Detailed discussion on the procedure employed to generate the random hole distribution can be found in Ref. [12]. The third lithographic step outlines the mesa structure and is then followed by dry inductively coupled plasma – reactive ion etching (ICP-RIE) process ($Cl/BCl_3/Ar$) to define the vertical sidewalls of the 10 μm thick laser mesa. Resonators having an area ranging from 0.06 to 0.18 mm^2 have been devised. Finally, a subsequent

ICP-RIE process allows removing the 800 nm thick highly doped capping layer inside the random holes.

In distinction to previous RL QCLs [9], we do not etch the holes all the way through the bottom of the active region, but only etch a shallow region into the gain medium. At the least, we etch 800 nm to remove the doped capping layer. In different fabrications, we etch the holes to different depths of 800 nm, 1.2, 1.5, and 1.8 μm, respectively. As a common characteristic, single-mode operation was obtained for smaller etch depths, and much richer multimode operation with progressively deeper etching. For the device presented here, we use a hole depth of 1.2 μm.

The device is then lapped to reduce the substrate thickness down to about 150 μm in order to allow stable operation in CW. Finally, devices are cleaved, mounted with an indium paste on a 1 mm thick bar of oxygen-free Cu that has 400 nm Au coating to improve thermal contact to the cryostat cold finger, and wire bonded.

A scanning electron microscope (SEM) image of a representative device is shown in Figure 1A. The resonator area is 0.06 mm^2. Figure 1B shows the light-current-voltage (L-I-V) characteristics collected at a heat sink temperature of 10 K, while driving the laser in pulsed operation with a pulse width of 1 μs and a duty cycle of 10, 40, and 80%, or under CW operation. In this latter case, the laser shows a maximum output power of 1.5 mW, a CW slope efficiency of about 40 mW/A and a wall plug efficiency of 0.5%.

To test if random lasers are sensitive to intracavity self-mixing effects, we use a reflector to feed the output THz radiation back onto the laser top surface. We then periodically change the external cavity length, while simultaneously monitoring variations induced in the voltage drop across the laser. To this purpose, we employ a Fourier transform infrared (FTIR) spectrometer to provide the feedback mechanism, employing the experimental set-up schematically sketched in Figure 2.

Typically, SM effects are retrieved by using a movable mirror, placed on a calibrated translation stage, to direct the light back into the laser cavity. In our case, we utilize the back reflection of the mirror in the moving arm of the Michelson interferometer of a FTIR spectrometer (Nicolet, Nexus 870) to feed back the light toward the random laser surface.

We use the output trigger of the FTIR as the trigger input to an oscilloscope (Tektronix DPO5204B) where we monitor the AC component of the voltage across the QCL. This ensures that the periodic mirror movement is synchronized with the waveform acquisition. Once the device is coarsely aligned to resolve the FTIR spectra, we fine-tune the alignment to maximize the SM signal. This allows simultaneously measuring both the spectra and SM signals with two different timescales: a slow movement over a long mirror distance is set to collect individual FTIR spectra, while a fast mirror velocity (3.17 mm/s) over a shorter distance, with 100 averages, is employed to trace the SM signals.

The resultant scattered field E_s is collected by a parabolic mirror and focused back onto the QCL surface along the same incident optical path, inducing changes in the QCL voltage (ΔV) (see details on the experimental arrangement in Figure 2). To quantify this properly, we relied on the well-established Lang-Kobayashi (LK) model [32]. In the very weak feedback limit, the voltage change at the QCL terminals can be written as:

$$\Delta V \propto s\cos\left(\omega_0 \frac{2L}{c} - \varphi\right) \tag{1}$$

where s and φ are the amplitude and phase, respectively, of the ratio between reflected and incident THz electric fields, $\omega_0 = 2\pi c/\lambda$ is the unperturbed laser frequency, and L is the varying laser-to-mirror distance. Since the RL is strongly sensitive to the backscattered field, we insert an attenuator (A) in the optical path to reduce the field intensity and

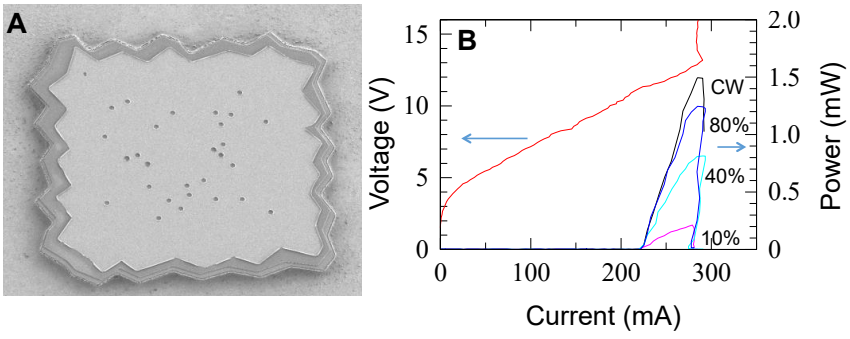

Figure 1: (A) Scanning electron microscope (SEM) image of the investigated random QCL resonator having an area of 0.06 mm^2, and patterned surface holes of 6 μm diameter. (B) Light-current (L-I) and voltage-current (V-I) characteristics as a function of the duty cycle or under CW operation measured on the device shown in panel (A), having area of 0.06 mm^2, hole diameter 6 μm and filling factor r/a = 11%, where r is the hole radius and a the average intersite distance defined as $a = L/N^{1/2}$, being N the number of holes and L the length of the average side of the patterned surface.

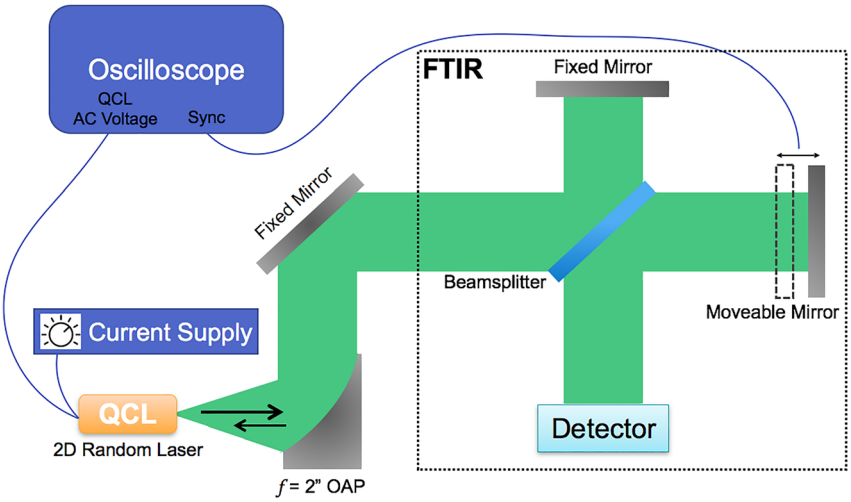

Figure 2: Diagram of self-mixing experimental setup. A Fourier transform infrared spectrometer (FTIR) simultaneously allows acquiring the emission spectra and measuring the self-mixing signal, by employing the mirror in the moving arm to vary the path-length for the light backscattered to the laser.

achieve a regime of very weak feedback in which the SM signal has a sinusoidal dependence on L, the system is kept in the validity of Equation (1), and the amplitude and phase components at the different demodulation orders can be directly retrieved with a standard fitting procedure [24]. In this regime, the proposed experimental layout is equivalent to a single-arm homodyne interferometer [16], in which the patterned random laser surface and the movable mirror define the external cavity of our self-mixing interferometer.

3 Self-mixing

As the external cavity length is changed, periodic fringes appear on the AC voltage signal. The FTIR movable mirror is displaced by a total length of 1.27 mm at a velocity $v_m = 3.17$ mm/s. From Equation (1), this leads to the periodic modulation of the laser voltage over time, with a period set by the QCL wavelength and by v_m. The knowledge of v_m provides a direct relation between the time traces recorded with the oscilloscope and the mirror coordinate. Figure 3A–E shows a selection of self-mixing waveforms as a function of time (bottom horizontal axis) measured at different driving currents; the corresponding FTIR spectra acquired at a heat sink temperature of 10 K in CW, are plotted in Figure 3F–L.

At the lower current (I = 236 mA), close to threshold, the SM is purely sinusoidal and the corresponding spectrum is single mode. By increasing the driving current, the self-mixing effect is still clearly visible. While progressively increasing the current, a set of modes at higher frequencies is excited and the random resonator reaches an overall spectral coverage of 340 GHz. When multiple modes are excited (Figure 3G–L), the SM waveform shows a visible beating between the different optical modes (Figure 3B–E).

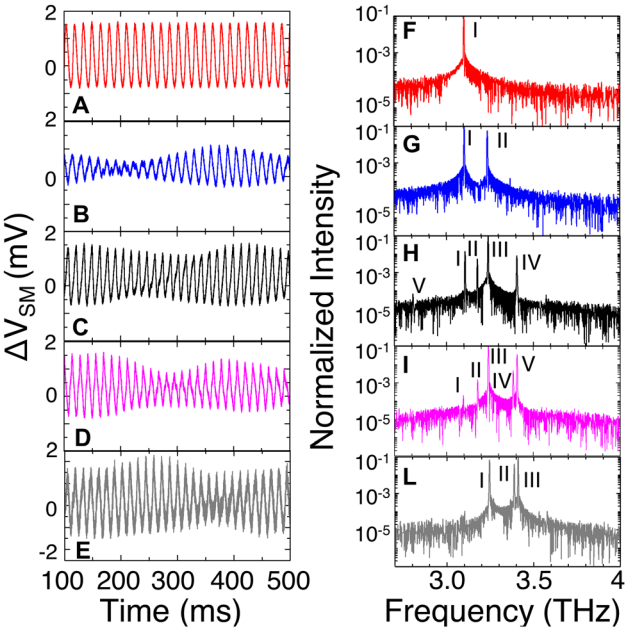

Figure 3: (A–E) Time evolution of the self-mixing traces collected with a fast oscilloscope (Zurich instruments, UHFLI Lock-in amplifier), while varying the position of the movable FTIR mirror and while driving the QCL with different currents: I = 236 mA; I = 250 mA; I = 260 mA, I = 275 mA, I = 284 mA (from top to bottom). (F–L) Corresponding FTIR emission spectra measured in rapid scan mode, while driving the random laser at a heat sink temperature of 10 K, and with currents I = 236 mA; I = 250 mA; I = 260 mA, I = 275 mA, I = 284 mA (from top to bottom), with a resolution of 0.075 cm^{-1}.

By increasing the current until the negative differential resistance region is reached, SM fringes persist (Figure 3E).

This unambiguously discloses the ability of the random laser to sense the backscattered light that can be coupled back through the random holes and sensed by the laser. This means that RLs can then simultaneously operate

as surface emitting sources and very sensitive and fast detectors; the self-mixing process is indeed inherently governed by the rapid timescales (ps) typical of the QCL intersubband transition processes.

To provide a concrete application of the observed physical phenomenon, we select a random QCL amongst the set of fabricated devices, to demonstrate THz near-field nanoscopy based on self-detection of the THz field scattered by a scattering near-field optical microscope (s-SNOM) [24]. In this technique, the THz light of the QCL is focused on the metallic tip apex of an atomic force microscope (AFM), which then acts as a back-scatterer and its radius of curvature determines the microscope optical resolution [33]. When the tip is brought in close proximity to the sample, the THz field that it back-scatters is affected by the near-field interaction with the sample, such that it contains information on the sample dielectric constant.

The random laser acts simultaneously as powerful source illuminating the AFM tip of the s-SNOM, and as phase-sensitive detector of the scattered field exploiting the fact that SM mechanism is sensitive to reinjection of portion of the emitted light as low as 10^{-6}. The interference between the output and back-scattered field perturbs the laser contact voltage such that by monitoring it, the scattered intensity is detected.

In the experiment, the PtIr-coated AFM tip, with 40 nm nominal radius, operates in tapping mode at a frequency $\omega_t = 80$ kHz, with tapping amplitude of the order of 200 nm. The amplitude of the scattered light, resulting from the near-field interaction with the sample, oscillates at the tapping frequency as a consequence of the strong-dependence on the sample-tip distance. The perturbation to the laser voltage V contains components at the harmonics of the tapping frequency $\omega_n = n\omega_t$ which are

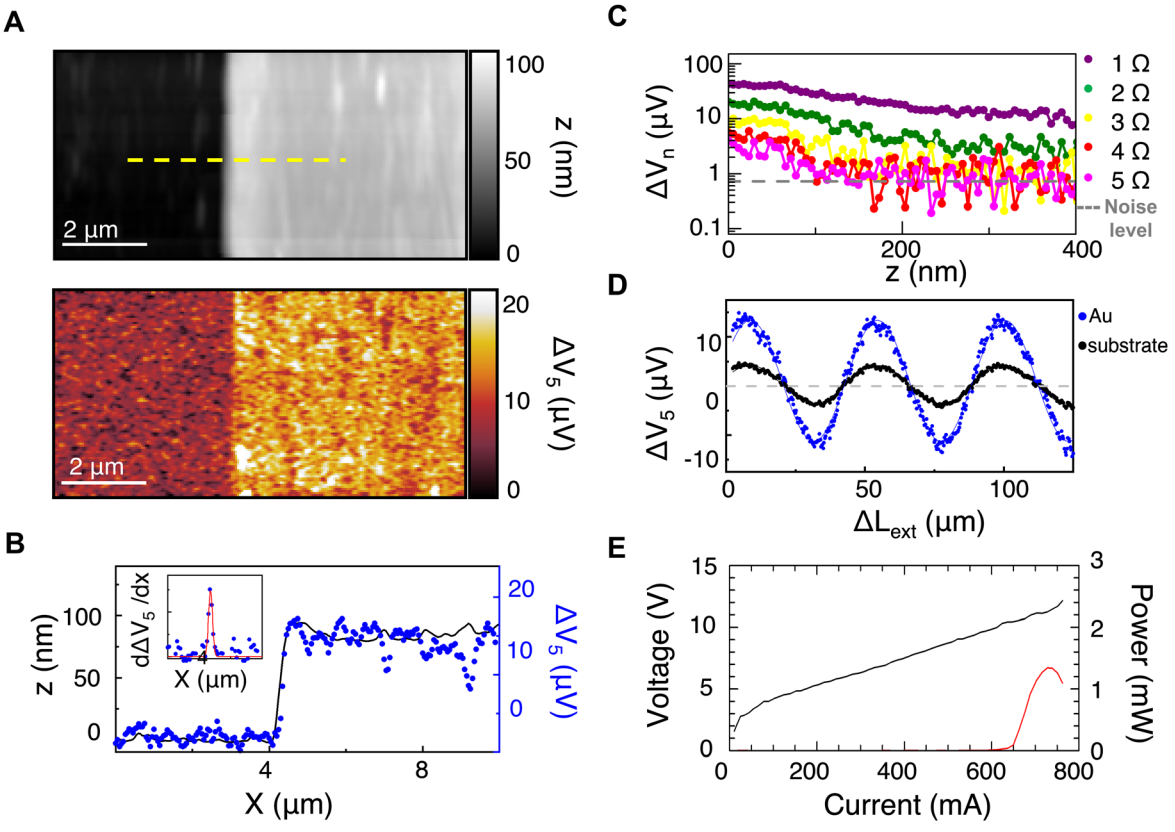

Figure 4: Near-field self-mixing measurements in single mode operation.
(A) (top panel) Sample topography (z) at the interface between 100 nm Au marker and undoped Si substrate and (bottom panel) self-mixing signal ΔV_5 demodulated at the fifth harmonics of the tapping frequency ω_t, collected with a speed of 2 µm/s corresponding to 6 ms per pixel; (B) line-profile along the yellow dashed line in panel (A) reporting the topography (black line-left axis) and the ΔV_5 signal (blue circles-right axis), including as inset the estimation of the spatial resolution (equal to 120 nm) from the Gaussian fit (red line) of the first derivative of the ΔV_5 (blue circles) at the sample edge; (C) approach curves for the self-mixing signal ΔV_n demodulated at the different harmonics order n; (D) self-mixing signal demodulated at the fifth harmonics as a function of the external cavity length L_{ext} at fixed point on the sample corresponding to Au (blue) and substrate (black) reporting data (circles) and sinusoidal fit (lines); (E) current-voltage and light-current characteristics acquired while driving the random laser in continuous wave at 10 K.

measured by lock-in detection up to the order $n = 5$. The demodulation allows isolating the near-field contribution from the background due to far-field illumination of the tip shaft and of the sample.

Figures 4A show the topography and the near-field maps collected on a gold marker, evaporated on an undoped Si substrate, while pumping it with a random laser having an area of 0.18 mm^2, a patterned set of holes having 6 µm diameter and filling factor $r/a = 18\%$, driven at $I = 640$ mA, while it emits a single frequency mode at 3.28 THz (black curve in Figure 5E). Here r is the hole radius and a the average intersite distance defined as $a = L/N^{1/2}$, where N the number of holes and L the average side of the patterned surface. The selected RL resonator shows a very low divergent (<15°) emission profile [12]. Due to the higher reflectivity, the Au marker gives a stronger scattering signal than that retrieved on the substrate, with the highest contrast obtained at the highest demodulation harmonics.

The moderately low signal-to-noise ratio (about 6.5 at the fifth demodulation order, Figure 4A, bottom panel) is an effect of the low scattering efficiency of the available commercial AFM probes whose length better fits with the source frequency (3.3 THz).

The overall spatial resolution is estimated from the analysis of the line profile across the edge of the marker, as shown in Figure 4B. The line spread function is best fit by a Gaussian function with a full width at half maximum (FWHM) of 120 nm, corresponding to approximately $\lambda/1000$, far below the limit imposed by diffraction, opening application to nanosize samples as well as to regimes of strong light confinement and strong light–matter interaction.

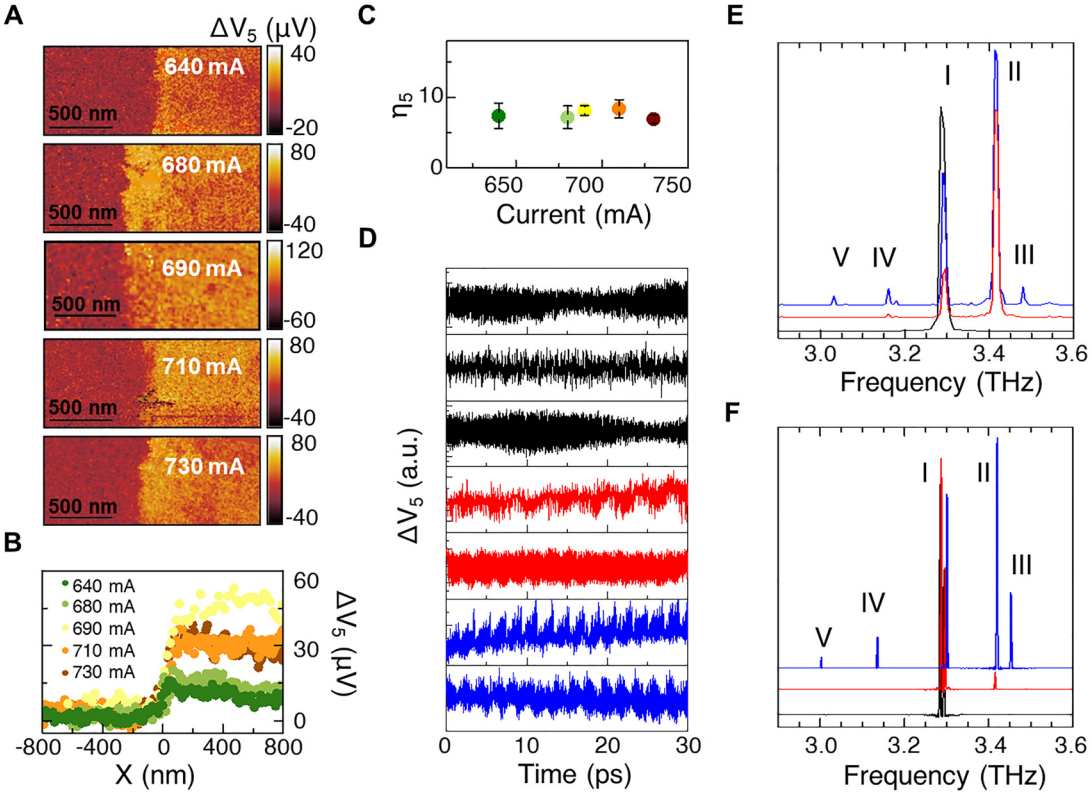

Figure 5: Near-field self-mixing measurements at various applied current.
(A) Self-mixing signal ΔV_5 demodulated at the fifth harmonics of the tapping frequency ω_t, collected while varying the driving laser current. (B) Line profile of the ΔV_5 signal along the Au-substrate interface, extracted from the maps of panel (A), by averaging vertically for 40 nm and corresponding to different driving currents ranging from 640 to 730 mA. (C) Signal contrast η_5 evaluated as the ratio between the average ΔV_5 signals from Au and from the substrate, determined from the line profiles in panel (B), showing constant value with the driving current. (D) Time evolution of the self-mixing traces collected with a fast lock-in amplifier (Zurich instruments, UHFLI Lock-in amplifier), while varying the laser to tip distance L_{ext} (L in Eq. (1)) and while driving the QCL with different currents: (from top to bottom) $I = 640$ mA; $I = 660$ mA; $I = 680$ mA; $I = 690$ mA; $I = 700$ mA; $I = 710$ mA; $I = 730$ mA. The resolution is given by the minimum displacement, that is 100 nm, which corresponds to a minimum time delay (i.e., temporal resolution) of about 0.3 fs. (E) Emission spectra retrieved while Fourier transforming the self-mixing traces of panel (D) collected at $I = 640$ mA, $I = 690$ mA and $I = 730$ mA (from bottom to top). (F) FTIR measurements in the far-field which agree well with the near-field spectra obtained from the SM fringes (from bottom to top).

The near-field nature is testified by the vanishing signal as the tip is retracted from the sample, as can be seen by looking to the approach curves shown in Figure 4C. The vertical confinement of the field can be quantified by the tip-to-sample distance at which the signal halves, which is equal to 100 nm in the case of the fifth harmonic.

Note that the higher spatial resolution retrieved in the present experiment with respect to Ref. [24] is an effect of the use of a different AFM tip that better matches the 3.3 THz impinging frequency.

Figure 4D shows the self-mixing signal, demodulated at the fifth harmonic, plotted as a function of the variation of L_{ext} (ΔL_{ext}) acquired at two fixed positions: on the Au marker and on the substrate. The curves are retrieved by inserting an optical delay line along the optical path that varies the length L_{ext} of the external cavity defined as the distance between the AFM tip and the laser top surface. Since the RL is strongly sensitive to the backscattered field, we insert an attenuator along the optical path to reduce the field intensity and achieve a regime of very low feedback in which the SM signal has a sinusoidal dependence on L_{ext}.

We unveil a visible increase of the amplitude of the SM fringes on gold with respect to those on the silicon substrate. On the other hand, no relative phase shift is detected. Indeed, strong phase changes are expected only for materials showing tip-induced near-field plasmonic or polaritonic resonances [33, 34], which is not the case for both gold and silicon in the 3–3.5 THz [35]. The lack of any phase-shift is also a signature of the phase-stability of the technique to spatial scanning of the sample and to any possible drift of the temperature, which during the experiments is kept constant within 0.1 K.

We then collect a set of near-field maps while progressively increasing the driving laser current (Figure 5A), following the light-current-voltage-characteristic (Figure 4E) of the RL. A stable self-mixing signal, up to high demodulation orders, can be retrieved, signature of the fact that even when the laser turns in a multimode regime and the feedback regime changes [15–17], the random resonator efficiently senses the backscattered light. From the line profile of the ΔV_5 signal, collected along the Au-substrate interface (Figure 5B) while driving the RL at different CW currents, we see a driving current-independent change of the amplitude contrast η_5 (Figure 5C) evaluated as the ratio between the average ΔV_5 signals from Au and from the substrate, which only depends on the dielectric properties of the two materials. The interference pattern of the corresponding self-mixing traces is investigated by varying L_{ext}. Figure 5D shows, in agreement with the far-field experiment of Figure 3, the beating between the different emitted optical modes with a visible transition between a condition of single mode emission (upper two black traces), to a condition of a dual mode emission (red traces) and, finally, a richer sequence of modes (blue traces). By Fourier transforming the collected near field self-mixing traces we can spectrally resolve the emission of the random laser, nicely reproducing the bias-dependent transition between a single mode, a dual mode or a multimode (up to 9 modes) emission (Figure 5E).

The extrapolated spectra are then compared with the FTIR emission spectra, measured under vacuum in a FTIR spectrometer (Bruker Vertex 80). Despite the resolution of the spectra retrieved from the self-mixing signal cannot match the 0.075 cm^{-1} spectral resolution of the FTIR due to the smaller sampled L_{ext} range, a good agreement between the spectral position of each emission peak (Figures 5E–F) is found, with the exception of the peak labeled I (Figure 5E) that is instead the convolution of two peaks spectrally separated by 8 GHz (Figure 5E). This starts to be visible in the bottom black trace in Figure 5D, where a small beating effect can be identified in the self-mixing traces.

Such a comparison discloses the potential of our detectorless near-field microscope to simultaneously trace near-field maps and capture the spectral position of the random modes, with a resolution level set by the total length of the scan of the self-mixing traces in the time domain.

4 Conclusions

In conclusion, we demonstrate that bi-dimensional random laser resonators can efficiently sense the light backscattered through a surface patterns of holes, simultaneously operating as THz detectors, through the self-mixing effect. The latter effect is then exploited to perform near-field optical nanoscopy in a detectorless s-SNOM system demonstrating sensitivity up to fifth harmonic of the demodulated signal with 120 nm spatial resolution. The demonstrated spatial resolution and the field confinement depend on the scattering probe shape and on the dielectric contrast of sample portions. The performances of our setup then match the state-of-the art THz s-SNOM facilities based on spatially coherent sources [24, 29, 36].

The time evolution of the self-mixing traces is also here exploited to retrieve the bias dependent spectral emission of the random laser and to provide a clear demonstration of the random laser sensitivity to the self-mixing effect under different operational conditions, i.e., from a very weak feedback regime (I = 640 mA), conventionally exploited in self-mixing interferometry [16, 17, 31], to a weak feedback

regime (I = 660 mA – 690 mA) and then to the regime of very high feedback (I > 700 mA), characterized by a larger value of the Acket's parameter C. This capability is particularly promising given the tunability with driving current of the emitted spectrum, that here allows up to 340 GHz spectral coverage. The achieved results open new routes for both fundamental physics and application perspectives, including direct approaches to retrieve the temporal coherence and the intrinsic linewidth [37] of random lasers, speckle free nano-imaging, quantum metrology, display applications taking advantage of the angular distribution of the random laser output, sensing and medical diagnostics.

Acknowledgments: The authors acknowledge fruitful scientific discussions with Gaetano Scamarcio.
Author contributions: All the authors have accepted responsibility for the entire content of this submitted manuscript and approved submission.
Research funding: The authors acknowledge financial support from the ERC Project 681379 (SPRINT).
Conflict of interest statement: The authors declare no conflicts of interest.

References

[1] R. M. Balachandran, N. M. Lawandy, and J. A. Moon, "Theory of laser action in scattering gain media," *Opt. Lett.*, vol. 22, pp. 319–321, 1997.
[2] D. S. Wiersma, "The physics and applications of random lasers," *Nat. Phys.*, vol. 4, pp. 359–367, 2008.
[3] H. Cao, J. Y. Xu, D. Z. Zhang, et al., "Spatial confinement of laser light in active random media," *Phys. Rev. Lett.*, vol. 84, p. 5584, 2000.
[4] B. Redding, M. A. Choma, and H. Cao, "Spatial coherence of random laser emission," *Opt. Lett.*, vol. 36, pp. 3404–3406, 2011.
[5] N. M. Lawandy, R. M. Balachandram, A. S. L. Gomes, and E. Sauvain, "Laser action in strongly scattering media," *Nature*, vol. 368, pp. 436–438, 1994.
[6] C. Gouedard, D. Husson, C. Sauteret, F. Auzel, and A. Migus, "Generation of spatially incoherent short pulses in laser-pumped neodymium stoichiometric crystals and powders," *J. Opt. Soc. Am. B*, vol. 10, pp. 2358–2362, 1993.
[7] Q. Song, S. Xiao, Z. Xu, et al., "Random lasing in bone tissue," *Opt. Lett.*, vol. 35, pp. 1425–1427, 2010.
[8] H. K. Liang, B. Meng, G. Liang, et al., "Electrically pumped mid-infrared random lasers," *Adv. Mater.*, vol. 25, pp. 6859–6863, 2013.
[9] S. Schoenhuber, M. Brandstetter, T. Hisch, et al., "Random lasers for broadband directional emission," *Optica*, vol. 3, pp. 1035–1038, 2016.
[10] Y. Zeng, G. Liang, H. K. Liang, et al., "Designer multimode localized random lasing in amorphous lattices at terahertz frequencies," *ACS Photonics*, vol. 3, pp. 2453–2460, 2016.
[11] Y. Zeng, G. Liang, and B. Qiang, "Two-dimensional multimode terahertz random lasing with metal pillars," *ACS Photonics*, vol. 5, pp. 2928–2935, 2018.
[12] S. Biasco, H. E. Beere, D. A. Ritchie, et al., "Frequency-tunable continuous-wave random lasers at terahertz frequencies," *Light Sci. Appl.*, vol. 8, p. 43, 2019.
[13] L. Salemi, K. Garrasi, S. Biasco, et al., "One-dimensional, surface emitting, disordered Terahertz lasers," *APL Photonics*, vol. 5, p. 036102, 2020.
[14] M. Leonetti, C. Conti, and C. Lopez, "The mode locking transition of a random laser," *Nat. Photonics*, vol. 5, pp. 615–617, 2011.
[15] H. Cao, Y. Ling, J. Y. Xu, C. Q. Cao, and P. Kumar, "Photon statistics of random lasers with resonant feedback," *Phys. Rev. Lett.*, vol. 86, p. 4523, 2011.
[16] G. Giuliani and S. Donati, "Laser interferometry," in *Unlocking Dynamical Diversity*, Hoboken, USA, John Wiley & Sons, Ltd, 2005, pp. 217–255.
[17] T. Taimre, M. Nikolić, K. Bertling, Y. L. Lim, T. Bosch, and A. D. Rakić, "Laser feedback interferometry: a tutorial on the self-mixing effect for coherent sensing," *Adv. Opt. Photonics*, vol. 7, pp. 570–631, 2015.
[18] F. P. Mezzapesa, L. L. Columbo, M. Brambilla, et al., "Intrinsic stability of quantum cascade lasers against optical feedback," *Opt. Express*, vol. 21, pp. 13748–13757, 2013.
[19] F. P. Mezzapesa, L. L. Columbo, M. Brambilla, M. Dabbicco, M. S. Vitiello, and G. Scamarcio, "Imaging of free carriers in semiconductors via optical feedback in terahertz quantum cascade lasers," *Appl. Phys. Lett.*, vol. 104, p. 041112, 2014.
[20] Y. J. Han, J. Partington, R. Chhantyal-Pun, et al., "Gas spectroscopy through multimode self-mixing in a double-metal terahertz quantum cascade laser," *Opt. Lett.*, vol. 43, pp. 5933–5936, 2018.
[21] P. Dean, Y. L. Lim, A. Valavanis, et al., "Terahertz sensing and imaging through self-mixing in a quantum cascade laser," *Opt. Lett.*, vol. 36, pp. 2587–2589, 2011.
[22] F. P. Mezzapesa, L. L. Columbo, C. Rizza, et al., "Photo-generated metamaterials induce modulation of CW terahertz quantum cascade lasers," *Sci. Rep.*, vol. 5, p. 16207, 2015.
[23] F. P. Mezzapesa, M. Petruzzella, M. Dabbicco, et al., "Continuous-wave reflection imaging using optical feedback interferometry in terahertz and mid-infrared quantum cascade lasers," *IEEE Trans. Terahertz Sci. Technol.*, vol. 4, pp. 631–633, 2014.
[24] M. C. Giordano, S. Mastel, C. Liewald, et al., "Phase-resolved terahertz self-detection near- field microscopy," *Opt. Express*, vol. 26, pp. 3430–3438, 2018.
[25] B. Redding, M. A. Choma, and H. Cao, "Speckle-free laser imaging using random laser illumination," *Nat. Photonics*, vol. 6, pp. 355–359, 2012.
[26] Y. Liu, W. Yang, S. Xiao, et al., "Surface-emitting perovskite random lasers for speckle-free imaging," *ACS Nano*, vol. 13, pp. 10653–10661, 2019.
[27] D. E. Tranca, S. G. Stanciu, R. Hristu, C. Stoichita, S. A. M. Tofail, and G. A. Stanciu, "High-resolution quantitative determination of dielectric function by using scattering scanning near-field optical microscopy," *Sci. Rep.*, vol. 5, p. 11876, 2015.
[28] A. A. Govyadinov, I. Amenabar, F. Huth, P. S. Carney, and R. Hillenbrand, "Quantitative measurement of local infrared absorption and dielectric function with tip-enhanced near-field microscopy," *J. Phys. Chem. Lett.*, vol. 4, pp. 1526–1531, 2013.

[29] A. Woessner, P. Alonso-González, M. B. Lundeberg, et al., "Near-field photocurrent nanoscopy on bare and encapsulated graphene," *Nat. Commun.*, vol. 7, p. 10783, 2016.
[30] E. A. A. Pogna, M. Asgari, V. Zannier, L. Sorba, L. Viti, and M. S. Vitiello, "Unveiling the detection dynamics of semiconductor nanowire photodetectors by terahertz near-field nanoscopy," *Light Sci. Appl.*, vol. 9, pp. 1–12, 2020.
[31] A. Adam, "Review of near-field terahertz measurement methods and their applications," *J. Infrared, Millim. Terahertz Waves*, vol. 32, pp. 976–1019, 2011.
[32] R. Lang and K. Kobayashi, "External optical feedback effects on semiconductor injection laser properties," *IEEE J. Quant. Electron.*, vol. 16, pp. 347–355, 1980.
[33] F. Keilmann and R. Hillenbrand, "Near-field nanoscopy by elastic light scattering from a tip," in *Nano-Optics and Near-field Optical Microscopy*, Zayats and A. D. Richards, Eds., Boston, London, Artech House, 2009.
[34] B. Knoll and F. Keilmann, "Infrared conductivity mapping for nanoelectronics," *Appl. Phys. Lett.*, vol. 77, p. 3980, 2000.
[35] W. L. Chan, J. Deibel, and D. M. Mittleman, "Imaging with terahertz radiation," *Rep. Prog. Phys.*, vol. 70, pp. 1325–1379, 2007.
[36] A. J. Huber, F. Keilmann, J. Wittborn, J. Aizpurua, and R. Hillenbrand, "Terahertz near-field nanoscopy of mobile carriers in single semiconductor nanodevices," *Nano Lett.*, vol. 8, pp. 3766–3770, 2008.
[37] M. C. Cardilli, M. Dabbicco, F. P. Mezzapesa, and G. Scamarcio, "Linewidth measurement of mid infrared quantum cascade laser by optical feedback interferometry," *Appl. Phys. Lett.*, vol. 108, p. 031105, 2016.